

## TEM investigation of dislocation microstructure of experimentally deformed silicate garnet

P. Cordier<sup>a,\*</sup>, P. Raterron<sup>a</sup>, Y. Wang<sup>b</sup>

<sup>a</sup> *Laboratoire de Structure et Propriétés de l'Etat Solide, URA CNRS 234, Université des Sciences et Technologies de Lille, 59655 Villeneuve d'Ascq Cedex, France*

<sup>b</sup> *Center for High Pressure Research and Department of Earth and Space Sciences, State University of New York at Stony Brook, Stony Brook, NY 11794-210, USA*

Received 21 November 1995; accepted 25 January 1996

---

### Abstract

Deformation experiments have been carried out on single crystals of garnet (Py<sub>25</sub> Al<sub>67</sub> Sp<sub>2</sub> Gr<sub>6</sub>) under high confining pressure ( $P = 6.5$  GPa) and temperature ( $T = 1440^\circ\text{C}$ ) in a multi-anvil apparatus. The high pressure sample assembly was designed so as to generate high differential stress. In one experiment, the differential stress was limited by a single crystal of San Carlos olivine (oriented along [010]) added on top of the specimen. Garnet crystals have been plastically deformed which shows that under our experimental conditions, garnet is ductile. The dislocation microstructure, analysed by transmission electron microscopy (TEM), suggests that both  $\frac{1}{2}\langle 111 \rangle\{110\}$  and  $\langle 100 \rangle\{110\}$  glide systems have been activated. Some dislocations appear to be dissociated. The observations of dislocation junctions and subgrain structures indicate that dislocation climb is enhanced under our experimental conditions.

---

### 1. Introduction

Knowledge of rheological properties of major constituents of the mantle is crucial in understanding the dynamics of our planet. Although significant efforts have been devoted to constrain rheology of olivine and pyroxenes, which are the major phases of the Earth's upper mantle (see for instance Bai et al., 1991 and Raterron et al., 1994 and references therein), experimental data on minerals stable in the deep mantle have been lacking due to the technical difficulties in conducting deformation experiments under very high pressures. Garnets are among the

most abundant minerals in the transition zone, between 410 and 660 km depths (e.g. Ringwood, 1991), and in subducted oceanic lithosphere (Irfune and Ringwood, 1987) at depths within the transition zone.

Garnets are often regarded as very strong minerals. Indeed, recent experimental studies suggest that garnets have a higher strength than major co-existing minerals (Ingrin and Madon, 1995; Karato et al., 1995). However, microstructural observations of natural garnets from various origins (Ando et al., 1993; Ji and Martignole, 1994) including very deep samples (Doukhan et al., 1994) show that under some circumstances, garnets have been really plastically deformed. The question is now whether garnet dominates or not the rheology of the garnet-rich assemblages in the transition zone. Studying the rheology

---

\* Corresponding author.

of garnets is thus of primary importance in understanding the dynamics of this region of the Earth.

The present study describes deformation experiments performed on silicate garnets with a multi-anvil high-pressure apparatus. A modified sample assembly designed to induce significant differential stress has been used. This experimental set-up does not allow quantitative strain–stress relations to be obtained. The emphasis will be put on dislocation microstructure characterization by transmission electron microscopy (TEM) and the understanding of physical processes of deformation under mantle pressure and temperature conditions.

## 2. Experimental procedure

### 2.1. Description of the samples

A natural, gem-quality, single crystal of garnet was used in the present study. Its structural formula determined by micro-analysis in the TEM (see below) is:  $\text{Py}_{25}\text{Al}_{67}\text{Sp}_2\text{Gr}_6$ . A low density of small (less than 0.1 mm in dimension) fluid and solid inclusions was observed within the crystal with the optical microscope prior to deformation. Samples for both infrared measurements and deformation experiments were cut from the inclusion-free part of the crystal. The hydroxyl content of our crystal was determined, by infrared spectroscopy (in the range  $3000\text{--}4000\text{ cm}^{-1}$ ), to be 0.015 wt%  $\text{H}_2\text{O}$ . The

integrated molar absorptivity used for this determination corresponds to the pyrope–almandine compositions:  $\epsilon_i = 300\text{ l mol}^{-1}\text{ cm}^{-2}$  (Aines and Rossman, 1984).

The starting garnet crystal was oriented by using the X-ray Laue technique and then cut into 2 or 4-mm-thick slices, the plane of the cut having a normal close to one of the  $\langle 110 \rangle$  axes. Two cylinders (2.2 mm in diameter) were cored from the slices. A single crystal of natural San Carlos olivine (Arizona, USA) was also oriented (within  $\pm 2^\circ$ ) by universal stage and X-ray Laue techniques. A cylinder was then cored along the [010] direction. Olivine and garnet cylinders were slightly shortened and polished (with  $3\text{-}\mu\text{m}$  alumina powder) to eliminate chipped faces and provide resistance against fracturing.

Two deformation experiments were performed: one on a 4-mm-length cylinder of garnet single crystal, and the other on a composite crystal consisting of two 2-mm-length cylinders of garnet and olivine joined end to end.

### 2.2. Deformation experiments

The deformation experiments were performed in a 2000-t Uniaxial Split-Sphere Apparatus (USSA-2000) which has been described previously (e.g. Remsberg et al., 1988). This apparatus can achieve pressures ( $P$ ) in excess of 9 GPa and temperatures ( $T$ ) up to  $1600^\circ\text{C}$  (for several hours) in the 18-mm

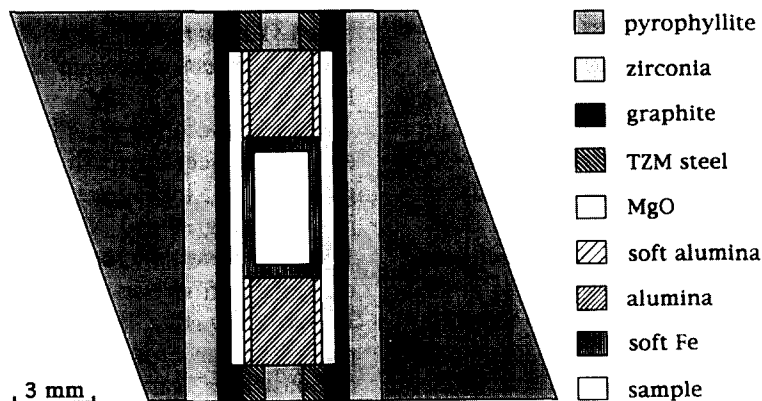


Fig. 1. Cross section of the 18/12 cell assembly used for the deformation experiments. This assembly utilizes an octahedron of edge length 18 mm which allows large volume sample experiments. The octahedron made of pyrophyllite, a good thermal insulator, is used for long run duration at high temperature. See text for further explanations.

cell assembly, for sample volumes of a few tens of cubic millimetres. Such apparatuses are mainly used for hydrostatic pressure experiments with cell assemblies designed to minimize differential stresses, which usually do not exceed 0.4 GPa (Wang et al., 1988; Ingrin and Liebermann, 1989). However, both Liebermann and Wang (1992) and Bussod et al. (1993) showed that a multi-anvil press can also be used as a high  $P$ – $T$  deformation apparatus. With this goal, we used the 18/12 pyrophyllite octahedron previously calibrated under pressure at room and high temperature; in order to strongly increase the differential stress within the cell assembly, we placed two non-machinable alumina rods, acting as pistons, on both ends of the sample.

Fig. 1 shows a cross-section of the high-pressure cell used (after modification): the cylindrical sample (garnet single crystal, or garnet–olivine composite crystal) is fitted into a soft iron capsule which mechanically seals during pressure increase at room temperature. The role of the Fe-capsule is to reduce the temperature gradient within the sample, and to chemically isolate the sample from any contamination. Iron is also a relatively soft material with a much lower mechanical resistance compared with alumina, thus preventing fracturing of the sample during cold compression. We also followed the recommendation of Bertran-Alvarez et al. (1992) who showed that the use of Fe-capsules for high  $T$ – $P$  experiments is an efficient method to maintain ferrous iron-bearing minerals within their redox stability fields. The Fe-capsule is lined by MgO which isolates the graphite heater from Fe metal and provides good thermal conduction. The external sleeve of the cell is made of zirconia which provides good thermal isolation from the outside, as well as the pyrophyllite octahedron surrounding the cell.

The  $P$ – $T$  conditions of the two experiments performed are given in Table 1. A typical  $P$ – $T$  path followed during the runs is illustrated in Fig. 2. Despite  $P$ – $T$  conditions near the graphite–diamond transition (see for instance Liu and Bassett, 1986), no characteristic decrease of the heater resistance was noticeable, even after 2 h at the peak temperature. No thermocouple was used during the run, as introduction of thermocouples increases the risk of producing fracturing in the sample during compression. The temperature was deduced from the mea-

Table 1

Annealing conditions

Sample label	Type <sup>a</sup> of crystal(s)	Pressure (GPa)	Central <sup>b</sup> temperature (°C)	Annealing duration (h:min)
2083	Gt	6.5 ± 0.3	1440 ± 45	2:00
2087	Gt/Ol	6.5 ± 0.3	1440 ± 45	0:55

<sup>a</sup> Symbols Gt and Ol stand for garnet and olivine, respectively.

<sup>b</sup> Thermal gradient from the centre to the ends  $\approx -140^\circ\text{C}$ .

surement of the power ( $W$ ) supplied to the heater and by using the calibration curves  $T = f(W)$  previously established at 6 GPa for this cell assembly. The uncertainty reflects reproducibility from run to run (J. Zhang and P. Raterron, personal communication, 1994). Zhang and Raterron also measured the thermal gradient along the assembly axis; from their measurement, we estimate that the temperature at the extremities of the sample at annealing conditions was about  $140^\circ\text{C}$  lower than the temperature at the centre of the sample. Taking into account both the temperature uncertainty and gradient we estimate that the temperature of any part of the sample at annealing conditions ranges from 1250 to  $1490^\circ\text{C}$ . At the end of the runs, the sample was quenched to room temperature, and the pressure slowly (for about 17 h) decreased to 1 atm in order to prevent fracturing of the sample during depressurization.

The differential stress and strain rate during the annealing are difficult to estimate in a multi-anvil

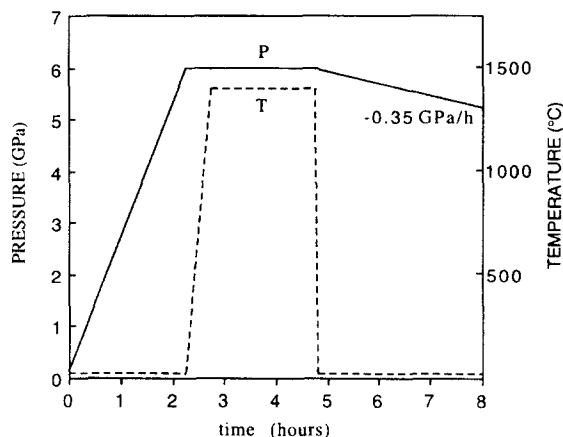


Fig. 2. Experimental procedure for a multi-anvil deformation experiment. Pressure versus time (solid line) and temperature versus time (broken line). See text for details.

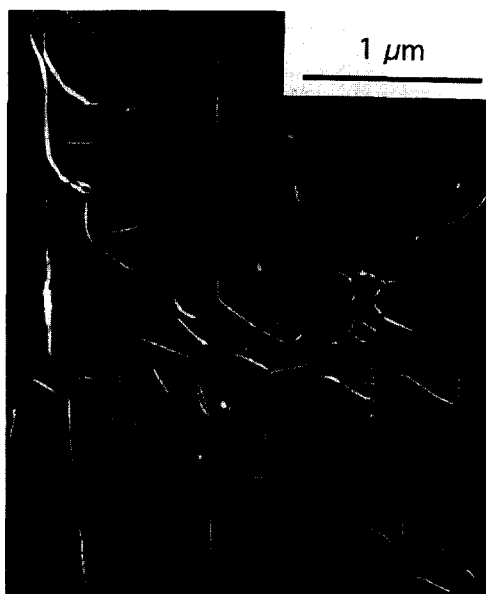


Fig. 3. Run #2083. Dislocations in glide configuration (arrowed). Weak-beam dark field micrograph.  $g$ : 420.

apparatus. Bussod et al. (1993) monitored the relative displacement of the apparatus guide blocks in order to deduce strain rate for the sample, and estimated the applied stress using grain size piezometry on the deformed samples. The purpose of our experiments was not to deduce any rheological law, but to characterize by TEM the active slip systems of silicate garnet; the applied stress and strain rate during the runs were not critical parameters. Run #2083 was performed on garnet single crystal alone and, as reported below, we observed that the sample #2083 deformed plastically during this experiment. Run #2087 was thus performed on a garnet–olivine composite crystal, in order to limit the deviatoric stress in the assembly to the flow stress of olivine (stressed along one of its hard orientations: [010]). When recovered, both the garnet and the olivine crystals were plastically deformed.

### 2.3. Transmission electron microscopy

Thin sections of the samples ( $\approx 20 \mu\text{m}$ ) were prepared by mechanical grinding and then optically polished on both faces with cerium oxide. Electron

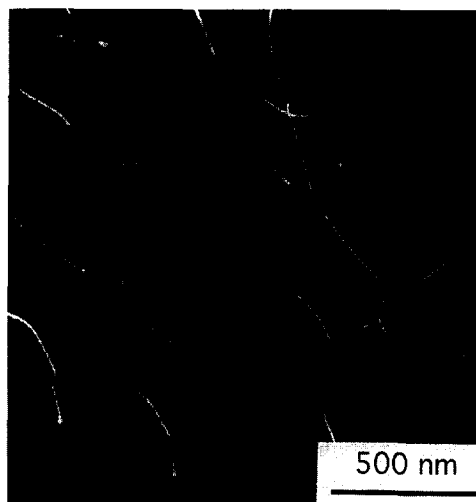


Fig. 4. Run #2083. Dislocations in climb configuration, junctions. Weak-beam dark field micrograph.  $g$ : 400.

transparent foils were finally obtained by ion milling at 5 kV under a low beam angle of  $15^\circ$ . TEM observations were carried out at 300 kV with a

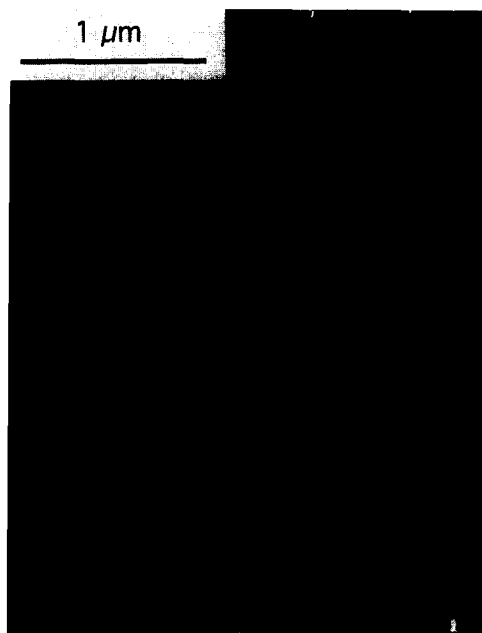


Fig. 5. Run #2083. Parallel subgrain boundaries (arrowed) in formation. Weak-beam dark field micrograph.  $g$ : 400.

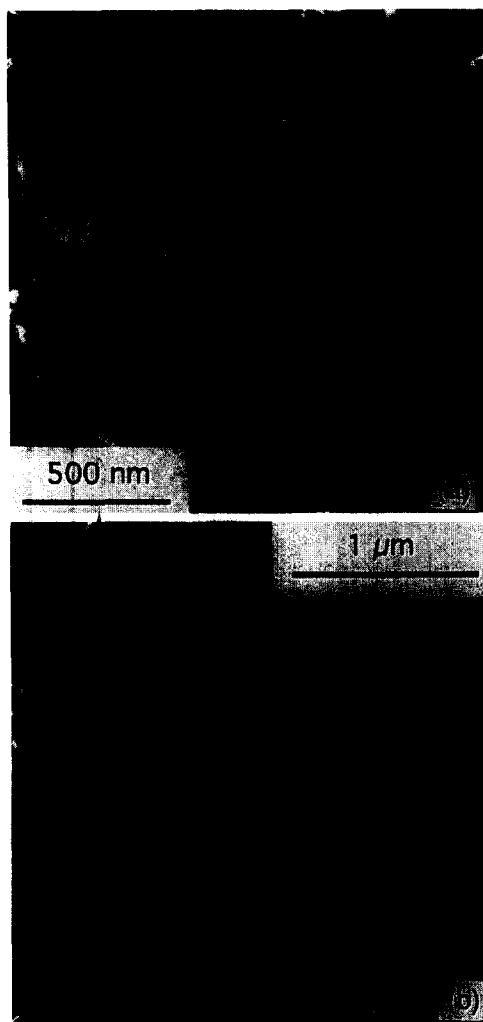


Fig. 6. Run #2083. Relaxed subgrain boundaries. (a) One dislocation family, pure tilt boundaries. (b) Two dislocation families, pure twist boundary. Weak-beam dark field micrographs.  $g$ : 400.

Philips CM30 microscope. Microanalyses in the TEM were performed with a Tracor energy dispersive X-ray attachment equipped with a Ge detector and an ultra-thin window allowing light elements such as oxygen to be detected.

As already noticed by several authors, characterization of dislocation Burgers vectors is difficult in the garnet structure (Rabier et al., 1976; Ando et al., 1993; Doukhan et al., 1994). The reason is the large unit cell which renders satisfactory two-beam

diffraction conditions difficult to obtain. It is thus delicate to use the conventional method of characterisation based on the  $g \cdot b = 0$  and  $g \cdot b \times u = 0$  invisibility criteria. Indeed, Ando et al. (1993) chose another method based on the Burgers circuit. Lattice fringes were counted on high resolution micrographs along a closed circuit enclosing the dislocation core. This method based on high resolution micrographs suffers, however, some limitation as it applies only to the special case where dislocations are viewed edge-on. Moreover, the Burgers vectors must be in the plane of the micrographs, otherwise the full Burgers vector cannot be determined. In the present study we have analysed the dislocations in garnet by large angle convergent beam electron diffraction: LACBED (Cherns and Preston, 1986; Tanaka et al., 1988; Cherns and Morniroli, 1994). LACBED has been applied recently in mineralogy to analyse dislocations in quartz (Cordier et al., 1995). In LACBED mode, when a dislocation intersects a Bragg line (i.e. the line where the exact Bragg condition is satisfied) with the diffraction vector  $g$ , the line splits into  $n$  nodes if  $g \cdot b = n$  (Cherns and Preston rule). If the dislocation line is long enough, then it is possible to place it with respect to the Bragg lines so that it crosses at least three Bragg lines. Three linear equa-

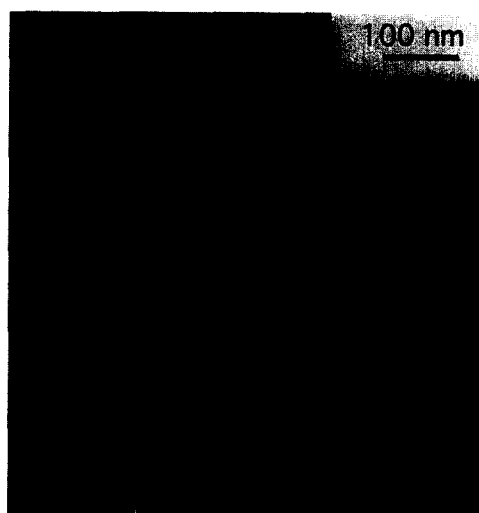


Fig. 7. Run #2083. Dissociated dislocation. Weak-beam dark field micrograph.  $g$ : 400.



tions of the type  $g_i \cdot b = n_i$  are obtained whose solution uniquely gives the Burgers vector. If the dislocation is too short, then it is successively placed on three Bragg lines and the Burgers vector is deduced as above. This method requires knowledge of:

- $n$ , the number of intensity minima in a dark field pattern,
- the direction of the dislocation line characterized by a unit vector  $u$ ,
- the  $hkl$  indices of the  $g$  Bragg line,
- the direction of the deviation parameter  $s$ .

These two last features are identified by comparisons with theoretical patterns drawn by means of a computer program, based on the kinematical theory, which was especially developed for this application.

### 3. Microscopic observations

#### 3.1. Garnet samples

The dislocation microstructures are very similar in samples from both #2083 and #2087 experiments. They will thus be described together. The dislocations distribution is rather heterogeneous in both samples. Some areas have not been deformed and are completely pristine. Some large areas, on the contrary, exhibit numerous dislocations. Dislocation densities between  $10^{12}$  and  $10^{13} \text{ m}^{-2}$  are routinely observed. Careful examination of the microstructure shows that different dislocation patterns can be distinguished. Some dislocations exhibit straight segments aligned along specific crystallographic orientations (Fig. 3): they are clearly confined in their glide plane. However, in most cases, the dislocation lines are curved and do not seem to belong to any specific plane. The dislocation lines are entangled and they often form junctions (Fig. 4). At some places, one can see dislocations which interact with each other and arrange themselves in subgrain boundaries to minimize total elastic energy of the crystal (Fig. 5). Fig. 6 shows a more advanced stage of recovery with relaxed subgrain boundaries. Such well-organized subgrain boundaries are common in our specimens. Careful observation in weak-beam dark field (WBDF) shows that some free dislocations are dissociated (Fig. 7, also see Discussion).

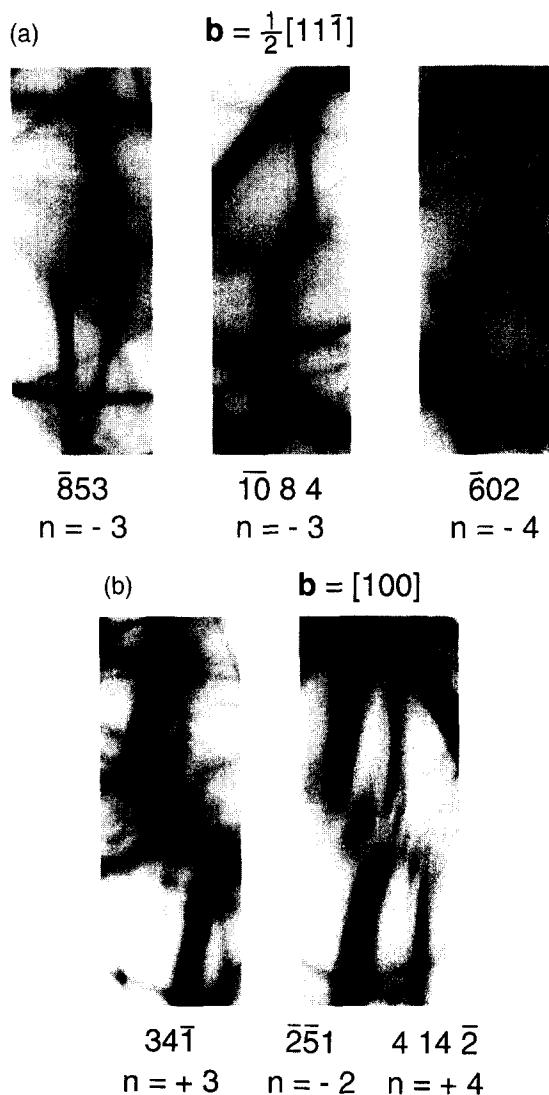


Fig. 9. LACBED analysis of dislocation Burgers vectors: (a) Case of a  $\frac{1}{2}[11\bar{1}]$  dislocation crossed with the  $\bar{6}02$ ,  $\bar{1}0\ 8\ 4$  and  $\bar{8}53$  Bragg lines. (b) Intersection of the  $4\ 14\ \bar{2}$ ,  $\bar{2}51$  and  $34\bar{1}$  Bragg lines with a  $[100]$  dislocation.

Dislocation Burgers vectors have been analysed by LACBED. Diffraction experiments have been carried out close to the  $[103]$  zone axis (Fig. 8). More than 40 dislocations have been fully characterized. Two-thirds of them are of the  $\frac{1}{2}\langle 111 \rangle$  type (Fig. 9(a)) and the rest are of the  $\langle 100 \rangle$  type (Fig. 9(b)). More precisely, we have found  $\frac{1}{2}[111]$ ,  $\frac{1}{2}[\bar{1}11]$ ,

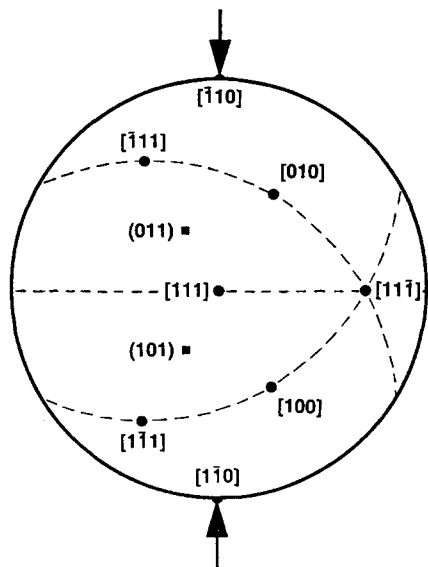


Fig. 10. Stereographic projection showing the Burgers vectors analysed (circles) in a single TEM thin foil from run #2087. Arrows indicate the compression axis.

$\frac{1}{2}[\bar{1}\bar{1}\bar{1}]$ ,  $\frac{1}{2}[\bar{1}\bar{1}1]$ ,  $[100]$  and  $[010]$  vectors. These results are summarized in Fig. 10 on a stereographic projection.

### 3.2. Olivine #2087

The microstructure is very heterogeneous in olivine too. Some regions are free of dislocations. Most of the crystal exhibits numerous free dislocations with densities ranging from  $10^{10}$  to  $5 \cdot 10^{13} \text{ m}^{-2}$ . Dislocation Burgers vectors have been analysed by means of the usual invisibility criteria. One finds  $\mathbf{b} = [100]$  and  $[001]$ . Straight screw  $[100]$  dislocation segments appear to be confined in the  $(010)$  plane.  $[001]$  dislocations have less preferential orientations. In dislocation-rich areas, dislocations form numerous subgrain boundaries. In some highly deformed zones, polygonization and recrystallization are well developed.

## 4. Discussion

The Burgers vectors of the stable dislocations in bcc structures are  $\frac{1}{2}\langle 111 \rangle$  and  $\langle 100 \rangle$ . These two

types of dislocations have already been found in deformed garnets (Rabier et al., 1976; Garem et al., 1982; Ando et al., 1993; Doukhan et al., 1994). However,  $\langle 100 \rangle$  dislocations may result from the attractive reaction of  $\frac{1}{2}\langle 111 \rangle$  dislocations following the reaction:

$$\frac{1}{2}[111] + \frac{1}{2}[\bar{1}\bar{1}1] \rightarrow [001].$$

Indeed,  $\langle 100 \rangle$  dislocations identified so far occur as short segments in junctions (Rabier et al., 1976; Garem et al., 1982; Doukhan et al., 1994) suggesting that  $\langle 100 \rangle$  slip may not be significantly activated. In contrast, Ando et al. (1993) found that  $\langle 100 \rangle$  slip is a dominant deformation mode in natural garnets from peridotites.

A significant part of the dislocations analysed in the present study is of the  $\langle 100 \rangle$  type. Does this mean that  $\langle 100 \rangle$  slip has been activated? In LACBED mode, dislocations are mainly detected through their effects on the Bragg lines. In principle, a shadow image is superimposed on the LACBED pattern, due to the defocus in the LACBED mode. In our diffraction experiments, the shadow contrast of dislocations was extremely faint and did not allow an easy control of the microstructure during characterization of dislocation Burgers vectors. It is thus difficult to guarantee that  $\langle 100 \rangle$  dislocations characterized are not junction products. However, characterization of short dislocation segments in junctions is delicate work and has not been performed and is very unlikely to occur by chance. Moreover, it appeared during LACBED analysis that some regions of the crystal was dominated by  $\langle 100 \rangle$  dislocations while some others contained mostly  $\frac{1}{2}\langle 111 \rangle$  type. Altogether, these elements suggest that  $\langle 100 \rangle$  slip has been activated in our experiments.

The lattice parameter of garnets is rather large resulting in large Burgers vectors. In the present case,  $|\mathbf{b}|_{1/2\langle 111 \rangle} = 0.91 \text{ nm}$  and  $|\mathbf{b}|_{\langle 100 \rangle} = 1.05 \text{ nm}$ . The dislocations energy which is proportional to  $\mu b^2$  ( $\mu$  is the shear modulus) is then large compared with most other minerals and one expects dislocation dissociation to occur in garnets, reducing the core energy. WBDF imaging is a suitable technique to investigate dissociation of dislocations because it produces much sharper images than conventional

bright- or dark-field imaging (which corresponds to a strongly diffracted beam with a small Bragg error). Under optimum conditions, WBDF can reach resolution levels in the 2–5 nm range (Sarikaya and Howe, 1992). In the case of garnets, these levels are difficult to reach. The diffraction vectors which are suitable for dislocation imaging are 400, 420 or 640 (their extinction distances, in almandine, are 135, 160 and 201 nm, respectively). The use of such diffraction vectors corresponds frequently to high  $g \cdot b$  products (3 or 4). In such cases, the dislocation image is broad, the intensity diffracted being approximately proportional to  $(g \cdot b)^2$ . Intensity profiles calculated using the kinematical theory show that for  $g \cdot b = 3$  and 4, a double image is produced (Hirsch et al., 1977) which is usually seen on bright- or dark-field images (close to the Bragg conditions). However, both images have markedly different intensities. The dislocation presented in Fig. 7 has been imaged by WBDF (with a large Bragg error); it exhibits two fine bright lines with similar intensities. This contrast cannot be attributed to a double image and those lines would thus correspond to two partial dislocations. The dissociation widths observed are in the range 10–15 nm. The imaging conditions of Fig. 7 correspond to a very low intensity which makes direct observation of these dislocations with the microscope very difficult. As a consequence, it has not been possible yet to perform LACBED determinations and WBDF observations on the same dissociated dislocation. Up until now, we do not know which dislocations ( $\frac{1}{2}\langle 111 \rangle$  or  $\langle 100 \rangle$ ) are dissociated. The only dissociated dislocations that have been reported so far are not mobile dislocations. Doukhan et al. (1994) found dissociated  $\langle 110 \rangle$  dislocations in subgrain boundaries. According to these authors, these dislocations were the product of junctions and rearrangements within the subgrain boundary. Allen et al. (1987) observed the dissociation of a  $\frac{1}{2}\langle 111 \rangle$  dislocation into two  $\frac{1}{4}\langle 111 \rangle$  partials which was interpreted as a grown-in defect. Moreover, no dissociation was reported by Ando et al. (1993) from their high resolution TEM analysis of mobile dislocations. More work is definitely needed to assess the fine core structure of mobile dislocations in garnets.

From a mechanical point of view, the control of the deformation parameters is still very crude in our experiments. During pressurization, the specimen is

subjected to high non-hydrostatic stresses. While the specimen is heated, plastic deformation occurs to relax these stresses in the specimen as well as in the surrounding materials of the assembly. Our deformation experiments are thus stress relaxation tests with a differential stress and strain-rate which decrease with time. Such experiments are not suitable for large deformations and it is not surprising that the microstructure remains heterogeneous in both experiments which were at the peak temperature for 1 and 2 h, respectively, as the major contribution to dislocation multiplication must arise from the beginning of the test. Run #2087 was designed to limit the differential stress on the garnet at the level of the flow stress of olivine oriented along [010]. The slip directions in olivine are [100], [001] and, to a lesser extent, [010]. When olivine is compressed along [010], the Schmid factor is zero for all slip systems. Dislocation glide is then theoretically precluded in such experiments. Indeed, deformation experiments performed under such conditions (Durham and Goetze, 1977) have shown that the creep rate is three orders of magnitude slower than those observed when easy glide can be activated. In principle, the only possible deformation mode for olivine in our experiments is pure climb of edge dislocation segments. Evidence of  $a$  glide in (010) has, however, been observed in our olivine specimen. This suggests that the stress field may be more complicated than expected and that stress analysis based on the Schmid law in terms of a simplified stress geometry may not be relevant. This is to be compared with the microstructure in garnets for which dislocations with Burgers vectors  $\frac{1}{2}[111]$  and  $\frac{1}{2}[\bar{1}\bar{1}1]$  have been indexed (Fig. 10). These dislocations correspond to slip systems with no or little resolved shear stress. (The Schmid factors of these slip systems are not exactly zero as suggested by the simplified representation of Fig. 10, because the compression axis is slightly off the  $[\bar{1}10]$  direction – approximately  $10^\circ$ .)

Although some dislocations appear to be confined in their glide planes, one observes pervasive evidence of dislocation climb: dislocation junctions, well-organized subgrain boundaries. This suggests that diffusion is efficient enough at  $1440^\circ\text{C}$  to enhance climb motion of dislocations. Dislocation climb is usually a slow and difficult process because it involves diffusion of point defects (multicomponent

diffusion in the case of garnets). Climb usually offers little contribution to the total deformation. However, this deformation mode is likely to control the deformation rate because it helps dislocations to overcome local obstacles. Climb also largely affects the restoration process. Rabier et al. (1981) suggested, however, that high temperature creep of YIG could involve pure climb motion of dislocations associated to Bardeen–Herring sources. Such a deformation mode could be an alternative explanation for the occurrence of  $\frac{1}{2}[111]$  and  $\frac{1}{2}[\bar{1}\bar{1}\bar{1}]$  dislocations.

## 5. Conclusion

In this study, we have shown that high-pressure high-temperature deformation experiments can be performed on silicate garnets in a multi-anvil apparatus. We have shown also that garnet is ductile under our experimental conditions:  $P = 6$  GPa,  $T = 1440^\circ\text{C}$  and high differential stress. TEM analysis of the dislocation microstructure suggests that both  $\frac{1}{2}\langle 111 \rangle$  and  $\langle 100 \rangle$  slip have been activated. Occurrence of dissociation of mobile dislocations is reported. Dislocation climb appears to contribute significantly to plastic deformation at  $1440^\circ\text{C}$ .

## References

- Aines, R.D. and Rossman, G.R., 1984. The hydrous component in garnets: pyrospites. *Am. Mineral.*, 69: 1116–1126.
- Allen, F.M., Smith, B.K. and Busek P.R., 1987. Direct observation of dissociated dislocations in garnet. *Science*, 238: 1695–1697.
- Ando, J., Fujino, K. and Takeshita, T., 1993. Dislocation microstructures in naturally deformed silicate garnets. *Phys. Earth Planet. Inter.*, 80: 105–116.
- Bai, Q., Mackwell, S.J. and Kohlstedt, D.L., 1991. High temperature creep of olivine single crystals 1. Mechanical results for buffered samples. *J. Geophys. Res.*, 96(B2): 2441–2463.
- Bertran-Alvarez, Y., Jaoul, O. and Liebermann, R.C., 1992. Fe–Mg interdiffusion at very high pressure and controlled oxygen fugacity: technological advances and initial data at 7 GPa. *Phys. Earth Planet. Inter.*, 70: 102–118.
- Bussod, G.Y., Katsura, T. and Rubie, D.C., 1993. The large volume multi-anvil press as a high P–T deformation apparatus. *Pure Appl. Geophys.*, 141(1): 579–599.
- Cherns, D. and Momioli, J.P., 1994. Analysis of partial and stair-rod dislocations by large angle convergent beam electron diffraction. *Ultramicroscopy*, 53: 167–180.
- Cherns, D. and Preston, A.R., 1986. Convergent-beam diffraction studies of crystal defects. In: *Proceedings Eleventh International Congress on Electron Microscopy*, Kyoto. Vol. 1, p. 721.
- Cordier, P., Momioli, J.P. and Chems, D., 1995. Characterization of crystal defects in quartz by Large-Angle Convergent-Beam Electron Diffraction. *Philos. Mag. A*, 72: 1421–1430.
- Doukhan, N., Sautter, V. and Doukhan, J.C., 1994. Ultradeep, ultramafic mantle xenoliths: transmission electron microscopy preliminary results. *Phys. Earth Planet. Inter.*, 82: 195–207.
- Durham, W.B. and Goetze, C., 1977. Plastic flow of oriented single crystals of olivine 1. Mechanical data. *J. Geophys. Res.*, 82(36): 5737–5753.
- Garem, H., Rabier, J. and Veyssière, P., 1982. Slip systems in gadolinium gallium garnet single crystals. *J. Mater. Sci.*, 17: 878–884.
- Hirsch, P., Howie, A., Nicholson, R., Pashley, D.W. and Whelan, M.J., 1977. *Electron Microscopy of Thin Crystals*. R.E. Krieger Publishing Co., Inc., Malabar, FL, 563 pp.
- Ingrin, J. and Liebermann, R.C., 1989. Deviatoric stress in a girdle-anvil type high pressure apparatus: effect on the quartz-coesite phase transformation. *Phys. Earth Planet. Inter.*, 54: 378–385.
- Ingrin, J. and Madon, M., 1995. TEM observations of several spinel–garnet assemblies: toward the rheology of the transition zone. *Terra Nova*, 7: 509–515.
- Irfune, T. and Ringwood, A.E., 1987. Phase transformations in primitive MORB and pyrolyte compositions to 25 GPa and some geophysical implications. In: Y. Syono and M.H. Manghnani (Editors), *High-Pressure Research in Minerals Physics*. Terra Scientific Publishing Company (TERRAPUB), Tokyo/American Geophysical Union, Washington, DC, pp. 231–242.
- Ji, S. and Martignole, J., 1994. Ductility of garnets as an indicator of extremely high temperature deformation. *J. Struct. Geol.*, 16: 985–996.
- Karato, S.I., Wang, Z., Liu, B. and Fujino, K., 1995. Plastic deformation of garnets: systematics and implications for the rheology of the mantle transition zone. *Earth Planet. Sci. Lett.*, 130: 13–30.
- Liebermann, R.C. and Wang, Y., 1992. Characterization of sample environment in a uniaxial split-sphere apparatus. In: Y. Syono and M.H. Manghnani (Editor), *High Pressure Research: Application to Earth and Planetary Sciences*. Terra Scientific Publishing Company (TERRAPUB), Tokyo/American Geophysical Union, Washington, DC, pp. 19–31.
- Liu, L.G. and Bassett, W.A. (Editors), 1986. *Elements, Oxides, and Silicates: High-Pressure Phases with Implications for the Earth's Interior*. Oxford University Press, New York, Clarendon Press, Oxford, pp. 36–37.
- Rabier, J., Garem, H. and Veyssière, P., 1976. Transmission electron microscopy determinations of dislocation Burgers vectors in plastically deformed yttrium iron garnet single crystals. *J. Appl. Phys.*, 47: 4755–4758.
- Rabier, J., Veyssière, P. and Garem, H., 1981. Dissociation of dislocation with  $a/2\langle 111 \rangle$  Burgers vectors in YIG single crystals deformed at high temperature. *Philos. Mag. A*, 44(6): 1363–1373.

- Raterron, P., Doukhan, N., Jaoul, O. and Doukhan, J.C., 1994. High temperature deformation of diopside IV: predominance of {110} glide above 1000°C. *Phys. Earth Planet. Inter.*, 82: 209–222.
- Remsberg, A.R., Boland, J.N., Gasparik, T. and Liebermann, R.C., 1988. Mechanisms of the olivine–spinel transformation in  $\text{Co}_2\text{SiO}_4$ . *Phys. Chem. Miner.*, 15: 489–493.
- Ringwood, A.E., 1991. Phase transformations and their bearing on the constitution and dynamics of the mantle. *Geochim. Cosmochim. Acta*, 55: 2083–2110.
- Sarikaya, M. and Howe, J.M., 1992. Resolution in conventional transmission electron microscopy. *Ultramicroscopy*, 47: 145–161.
- Tanaka, M., Terauchi, M. and Kaneyama, T., 1988. Convergent-Beam Electron Diffraction II. Kyoto, Jeol Ltd.
- Wang, Y., Liebermann, R.C. and Boland, J.N., 1988. Olivine as an in situ piezometer for high pressure apparatus. *Phys. Chem. Miner.*, 15: 493–497.